Isolating trabecular morphology to study bone damage

Isolating trabecular morphology to study bone damage

F Buccino[1]
[1] Department of Mechanical Engineering, Politecnico di Milano, Italy
Email: federica.buccino@polimi.it

Abstract. Bone structure is particularly complex and characterized by an intricate hierarchical architecture. Consequently, bone damage occurs at the multi-scale. Clinical applications typically analyze bone fractures at the macro-scale, but currently damage modes at lower scales are not fully understood yet. This research focuses on the understanding of meso-scale damage, characterized by a network of trabeculae of different thickness and spatial orientation. In order to isolate this articulated morphology, bone samples from porcine vertebrae are scanned through micro-computed tomography (micro-CT) and replicated by means of selective laser melting technique (SLM), obtaining Ti6Al4V specimens. This is particularly useful, because these samples are realized with a uniform material, permitting to isolate morphological features. The SLM samples, after a check of the internal morphology, are mechanically tested under static compression. The load-displacement curve shows a first linear elastic section, followed by a collapse of the structure. This behavior is similar to the one of porcine vertebrae. Starting from micro-CT volume reconstruction, three finite element models are implemented. A global preliminary model of the entire sample is developed and the area with the highest level of strain is identified. In order to understand the distribution of stresses and strains in the critical zone, a sub-region of the original cylinder is considered. The results of the simulations identify a homogeneous distribution of deformations over the entire geometry, with the exception of the region characterized by a thinning of the trabeculae, called the failure band of the sample. By implementing an additional sub-model, the most strained trabecula is identified as the critical location, causing the collapse of the structure. The numerical models are then validated by comparing the numerical and experimental stiffness. This will allow to perform further analyses by varying the trabecular architecture and quantitatively evaluate the effect of morphology.

1. Introduction

As a result of the increase in the average age of the population, bone pathologies have become a significant issue. One of the most common bone diseases is osteoporosis [1][2], characterized by increased bone fragility and causing annually more than 8.9 million fractures [3]. The deterioration of bone tissue and the alteration of bone microarchitecture may compromise bone strength and increase the risk of fractures [4]. The most affected sites are the pelvis and the spine [5]: this leads to an important morbidity and in some

cases it can cause mortality. This results in an enormous health, psycho-social and economic concern for the disease management [6]. More in depth, vertebral fractures are often associated with bedridden patients, that lose their autonomy, resulting in an increase in hospitalization numbers [7].

Clinical images such as Dual X-Ray Absorptiometry (DXA), Radiographies, etc. are a useful tool for the diagnosis of osteoporosis. In particular, DXA evaluates the Bone Mineral Density, a global parameter measuring the optical density per square centimeter of bone surface upon imaging [8]. However, BMD alone is a limited predictor of fracture risk and it has been demonstrated that there are almost 30% of unpredicted vertebral fractures [9] [10]. This could be explained by introducing the role played by bone quality parameter [11], i.e. morphological factors that contributes to fracture resistance independently from the bone mineral density.

A clearer identification of bone morphology especially at the complex trabecular meso-scale could be possible only with the support of high-resolution images techniques, such as the micro-computed tomography. This technique, often used in combination with computational finite element models [12] [13], leads to the visualization of bone morphology at different magnification levels. From these models it is possible to derive local mechanical parameters, such as local stress or strain levels, leading to a more precise identification of bone damage initiation site. With the aim of isolating trabecular bone morphology and demonstrating the effects of a deteriorated bone structure, preliminary attempts have been performed by Barack et al. [14]. They compare two 3D printed trabecular bones at different bone degeneration levels, observing that a slight decrease in volume fraction corresponds to a significant reduction in structural strength and stiffness. Nagaraja et al. [15] deepen the role of local mechanical parameters, understanding factors contributing to microdamage initiation and identifying local failure criteria for healthy and diseased trabecular bone.

In this context, the present work aims at replicating the trabecular morphology of a porcine vertebra, isolating its geometry in selective laser melting (SLM) specimens. SLM samples, differently from bone, are realized with a uniform material, permitting the isolation of morphological features. SLM samples are then scanned through the micro-CT and then tested under static compression. Computational models are developed in order to define the weakest local region.

2. Materials and Methods

In order to isolate the trabecular morphology and give a first hint in the definition of damage initiation sites and in particular in the role of the morphology on it, a combination of experimental and numerical approaches is performed. A general overview of the followed procedure is reported in figure 1.

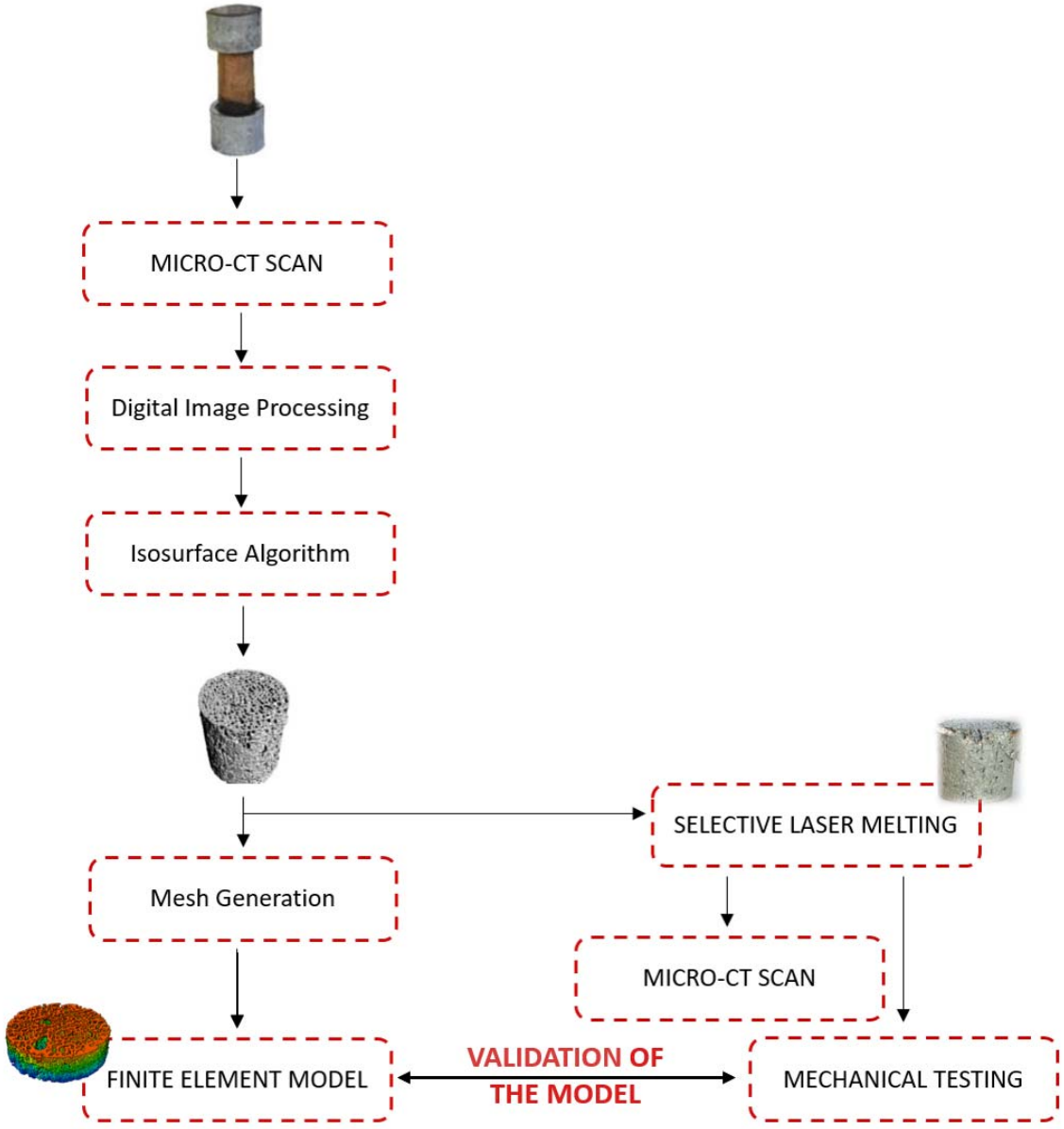

Figure 1. General workflow of the procedure

2.1. Experimental tests

2.1.1. Micro-CT scanning of porcine vertebra

A cylindrical specimen (1.3 mm in diameter and 1.5 mm in height) is obtained from the third porcine lumbar vertebra. A micro-CT scan with North Star Imaging 3D X-ray CT X25 tomographic system is performed in order to obtain a three-dimensional reconstruction of its volume, starting from single bi-dimensional projections. The following parameters are used for the scan:

- Resolution: 25.6 µm

- Voltage: 60 kV
- Current: 150 μA
- Number of projections: 1950

2.1.2. Porcine vertebra image analysis

After the micro-CT scan is performed on the porcine vertebra, a stack image of the digital volume is available and a segmenting procedure is performed. Image segmentation, typical in a set of medical images, helps to generate 3D reconstructions with the support of interpolation algorithms. With this aim, the open source software ImageJ Fiji is used, following specific steps:

- Setting of the dimensional scale;
- Selection and crop of the region of interest: the choice of different regions of interest and their dimensions will be detailed in paragraph 4;
- Filtration using a Gaussian Blur with a sigma of 1.5. The aim of this step is to reduce the noise, without altering the three-dimensional architecture of trabeculae. This is possible by performing a weighted average of the pixels in the neighborhood.
- Binarization using Otsu method with a local threshold for each image: this methodology is commonly used for the differentiation of tissues in tomographies [16]. It consists in the reduction of the within-class variance, by defining a threshold between foreground and background pixels. The threshold that gives the lower within-class variance is the binarization threshold, that leads to an image processing as the one reported in figure 2.

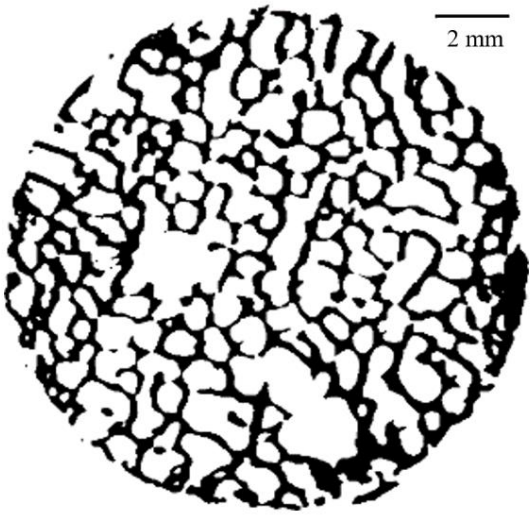

Figure 2. Binarized cross section of trabecular porcine sample

After the segmentation process, an isosurface is generated by exploiting the marching cubes' method for the construction of a triangular mesh, allowing a resampling of the digital volume. The resampling process set a value that smooths out small details. Resampling of 2, 4, 6 and 8 pixel units are considered. A resampling of 4 pixel units is finally used to build the mesh for the 3D printing (in Ti6Al4V) of the whole trabecular structure. The resampling of 4 pixel units shows the best compromise between low values of resampling, that lead to an accurate but less optimized mesh and high ones, that bring to lower accuracies. The influence on the resampling effect is shown in figure 3.

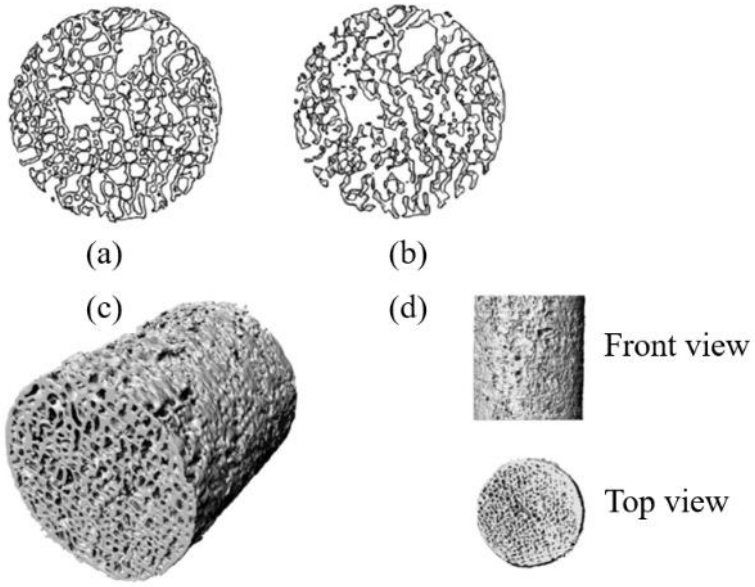

Figure 3. The effect of resampling 2 pixel units (a) and 8 pixel units (b) on the trabecular network. A loss in trabecular thickness is present in (b). A resampling of 4 pixel units is chosen for the final mesh generation (c). For resampling 4 pixel units the perspective, a top and front view is shown (d).

2.1.3. Selective Laser Melting of the porcine vertebra: morphology isolation
Starting from the .STL file generated from the micro-CT of the porcine vertebra, samples of titanium alloy (Ti6Al4V) are realized by means of Selective Laser Melting (SLM) technique at the laboratories of CNR-ICMATE in Lecco (Italy). The diameter and the height are the same of the trabecular bone, so 13 mm and 15 mm respectively. The SLM specimens are obtained by means of Renishaw AM 400 printing device with a scale 1:1. The realization technique, SLM, is an additive manufacturing technique that uses a laser source to melt metallic powders in the defined place with a high accuracy. The process parameters adopted for the specimens are reported in Table 1.

Power	Exposure Time	Layer thickness	Spot size	Point distance	Powder size
400 W	60 µs	60 µm	65 µm	80 µm	45 µm

Table 1. Process parameters for Ti6Al4V samples

2.1.4. Mechanical testing
Two SLM samples are tested under compressive loads using the MTS Alliance RF/150 uni-axial testing machine, equipped with a 100kN load cell. The tests are performed under displacement control with a speed of 1.60 mm/min. The selected outputs are the load with respect to the cross-head displacement. A deflectometer is inserted, so as to measure the upper plate vertical displacement with higher accuracy.

2.2. Numerical models and analyses

In combination with the experimental tests, numerical analyses are performed, starting from .STL files generated by micro-CT and used for SLM specimens. In order to obtain a solid mesh, the ShrinkWrap method is implemented: it is particularly suitable for complex geometries such as the trabecular network, because it is able to recognize the three-dimensional topology and then generate the mesh around it. The software Altair Hypermesh is used for meshing volumes of interest. The commercial solver ABAQUS is then used for analyses.

Compressive tests simulations are linear elastic. The Young modulus imposed is the one obtained from the experimental testing performed on SLM samples (E= 111597 MPa). The Poisson's ratio is 0.33 [17]. Hexahedral mesh is chosen over tetrahedral mesh since it is highly recommended for models that involves bone tissue [18]. Three different models are implemented, as reported in figure 4.

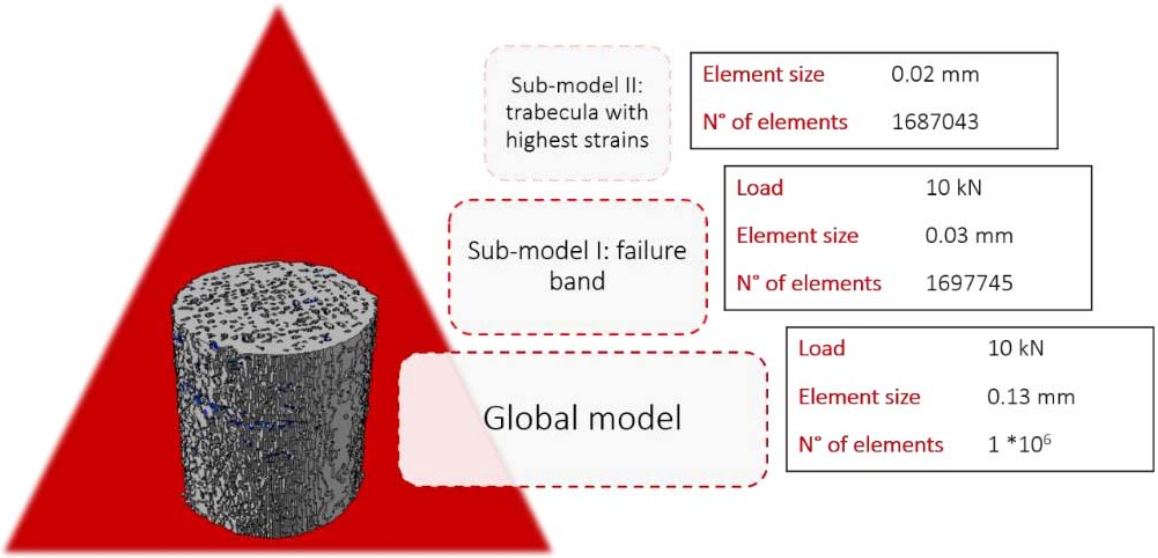

Figure 4. Overview of the three levels of magnification of the implemented computational models. On the right side the applied load, the element size and the number of elements present in the mesh is reported for the three models.

The global model and the first sub-model are loaded by a compressive force P=10 kN. The bottom surface is fully constrained, in order to simulate the experimental conditions.

The second sub-model is subjected to the displacements of the first sub-model.

3. Results

3.1. Experimental results

The output of micro-CT scan post-processing of both porcine and SLM samples is reported in figure 5.

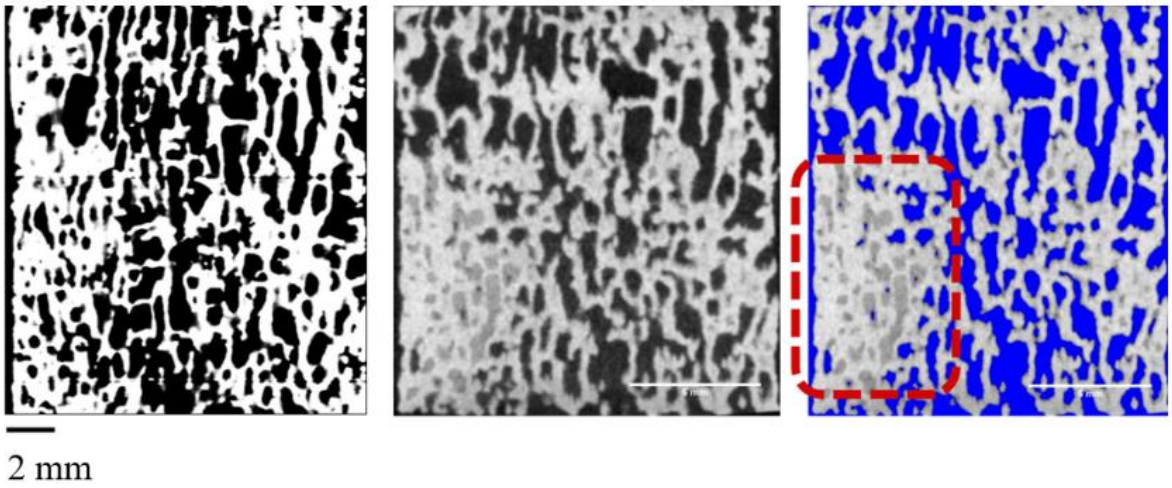

Figure 5. Micro-CT scan cross-section of porcine bone sample (a) and SLM specimen (b). In (c) a contrast enhancement is applied. Close cavities are highlighted by the red box.

Two different parameters are evaluated to determine if the SLM trabecular network is comparable with the porcine one: the degree of anisotropy (DA) and the Bone Surface (BS). The DA is a measure of how high the trabecular network is oriented within the volume of interest, computed by means of an iterative process. The BS is a parameter that evaluates the empty surfaces in a binarized region of interest.
The values are verified for each bi-dimensional section of the sample and then an average is reported in Table 2.

	Bone	**Ti6Al4V**	**Parameter variation**
DA	0.595	0.692	14.01%
BS	10432.4 mm^2	8743.3 mm^2	16.19%

Table 2. Comparison between the DA and BS in porcine sample and SLM specimen.

The variation between bone and SLM specimen's morphology, even if not significant, is due to some close cavities full of titanium alloy powder's residue. From DA and BS parameters it is possible to observe that the SLM specimen well reproduces the trabecular bone porcine structure.
As regards the mechanical response of SLM samples, two samples are tested under displacement control. The force-displacement graph of two SLM samples is reported in figure 6.

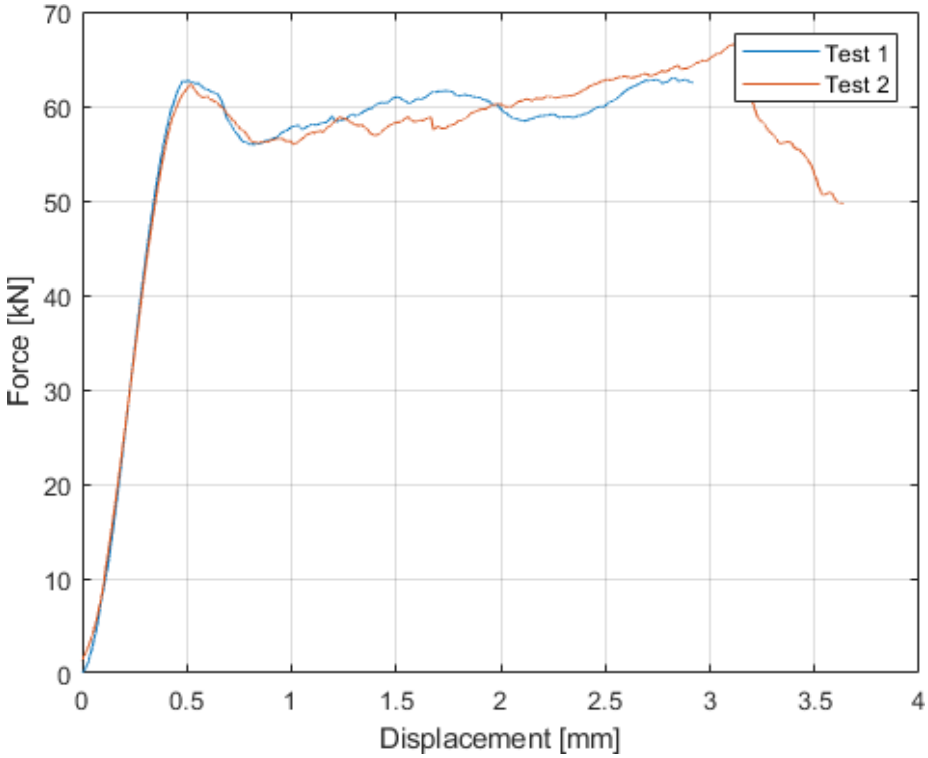

Figure 6. Force-displacement curves for two SLM samples.

The results show that the test is repeatable and at 0.5 mm displacement (end of the elastic zone) there is a peak in the force value, followed by a collapse of the structure. This reduction in the peak force is typical of trabecular bone structure's collapse. According to [19], trabecular structures may show three different curves (figure 7), but the majority of the considered specimens under compressive load show a behavior like II, that is similar to the one verified in SLM samples. This is an additional demonstration that SLM samples are able to replicate vertebral morphology.

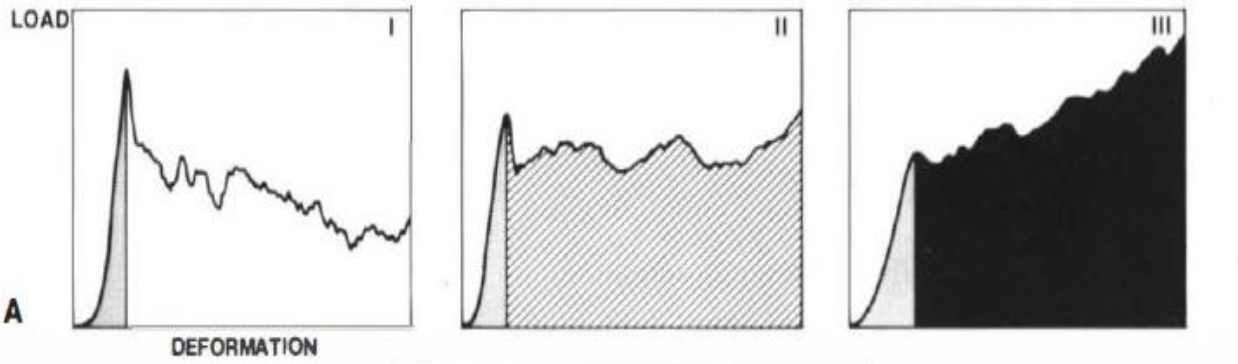

Figure 7. Mechanical behavior of trabecular bone in vertebrae.

The experimental stiffness is computed from figure 6 in the linear zone, removing the initial values for low values of displacement. The obtained value of stiffness is 192275 N/mm.

3.2. Numerical results

Numerical analyses, conducted in the linear elastic field, are implemented, in order to identify possible damage initiation sites.

From the global model, the maximum values of the local strains are extrapolated, as shown in figure 8. It is possible to identify a region characterized by higher local values of strain.

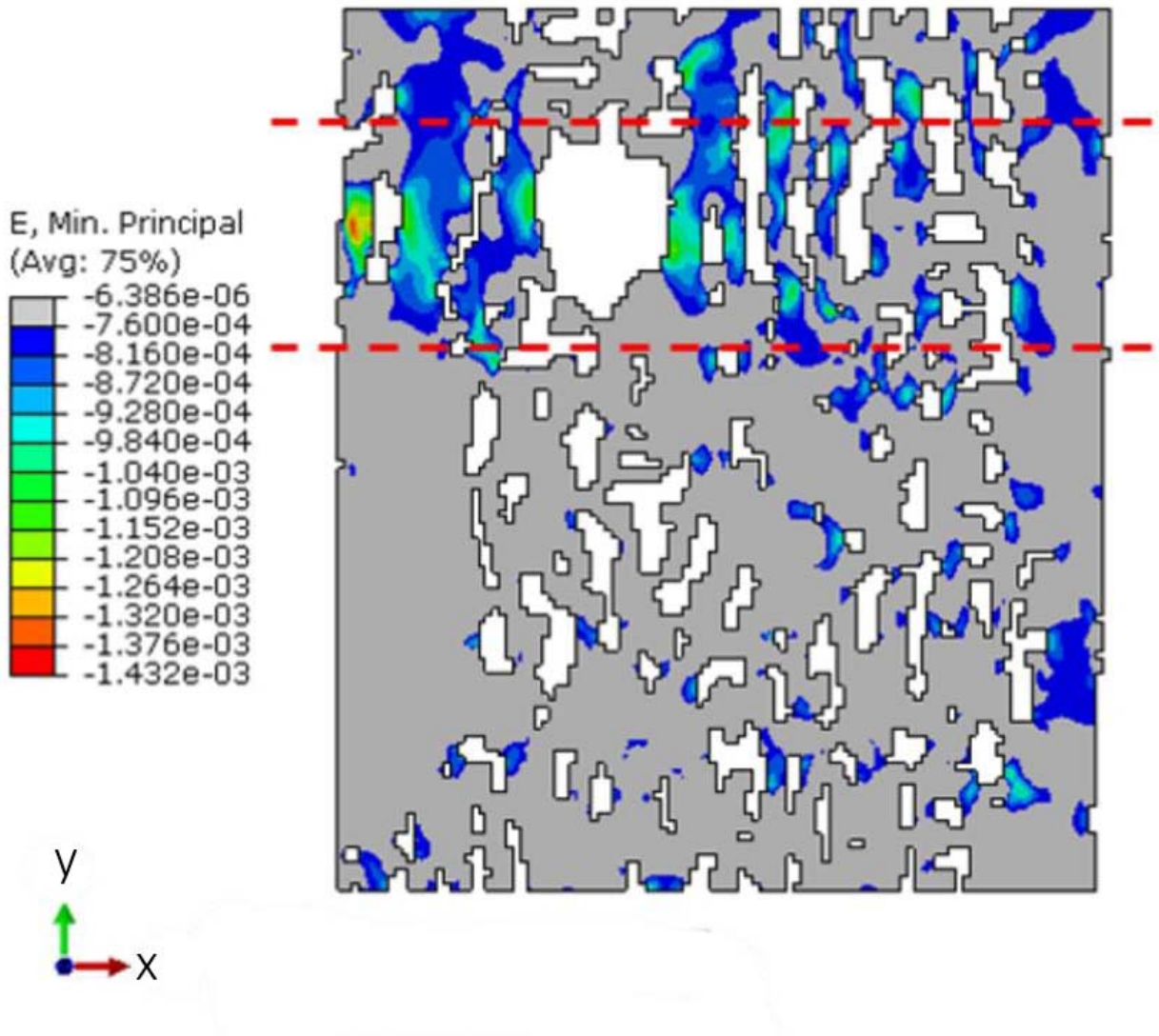

Figure 8. High strain zone highlighted in the global model. Section view in the Z-Y plane

This region (sub-model I) is considered with an improvement in the element size (0.03 mm instead of 0.13 mm), taking into account a 4 mm disk from the global model (figure 9) and identifies a volume defined "failure band". This corresponds to the zone characterized by the highest BS.

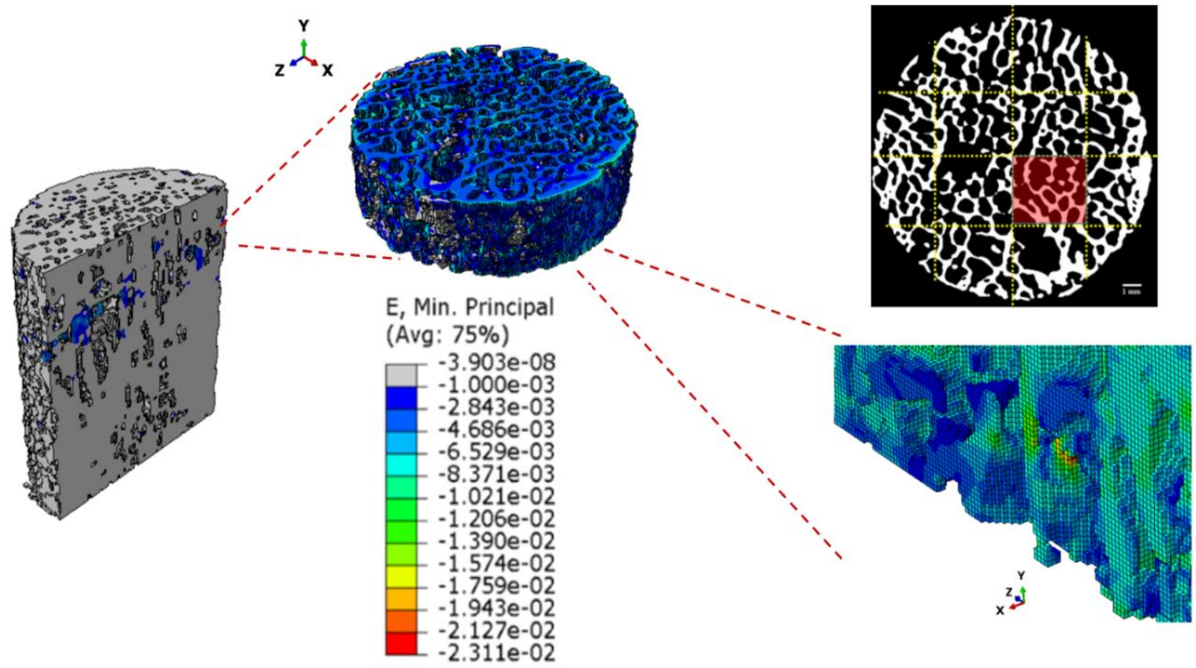

Figure 9. Sub-model I. The slice on the top right part highlights in red the location of the most loaded trabecula.

From the results of the second sub-model, it figures out that large strains are highly localized and, in the most strained zones, one of the most loaded trabeculae is identified.
From the first sub-model, a homogeneous division of 3mm x 3mm x 4mm is performed and sub-model II is generated (figure 10).

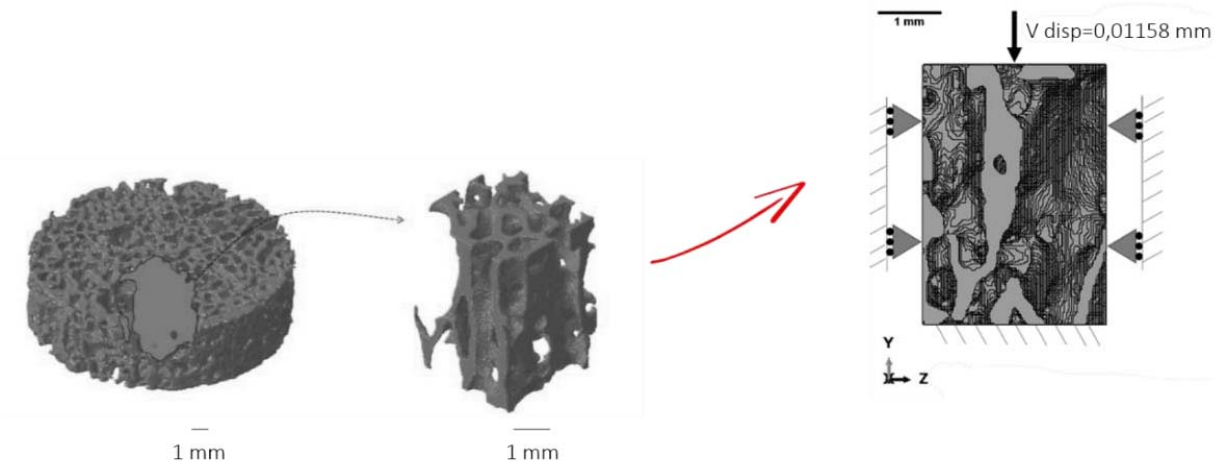

Figure 10. Sub-model II, identification of the sub-region.

The obtained results in terms of maximum values of local strains are highlighted in figure 11.

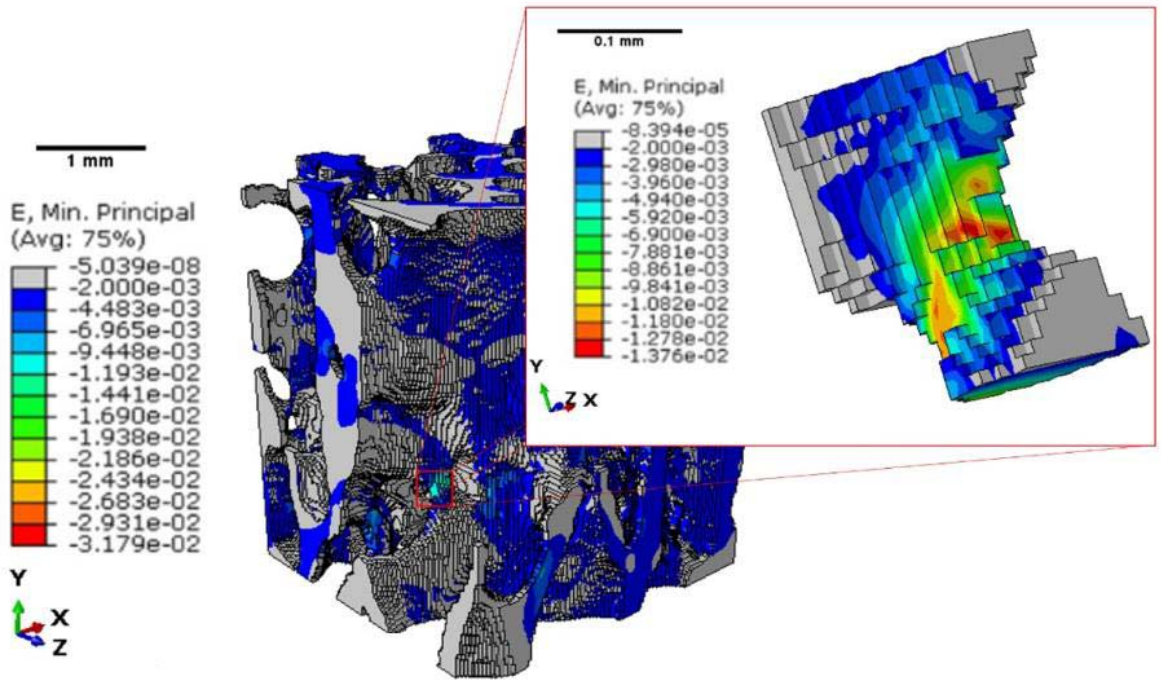

Figure 11. Sub-model II results.

4. Discussion and conclusion

The intrinsic value of the three implemented model resides in their ability to identify a region where damage is prone to start and more in detail the trabecula subjected to the highest strain. In addition to this, a validation of the model is performed, by comparing the numerical stiffness with the one obtained from experimental testing. The stiffness predicted by the global finite element model is equal to S(FEM)=160834 N/mm. Since trabecular structure models are very sensitive to the element size, a Richardson extrapolation [20] is performed to estimate the stiffness predicted by the computational model after a linear fitting of stiffness values obtained at element size of 0.13, 0.14 and 0.15 (figure 12). This linear fitting allows to dissociate the obtained computational stiffness from the element size of the mesh [21]. This approach has some limitations related to the low number of simulations carried out for refined meshes, but it represents the best compromise in terms of accuracy and computational costs [21].

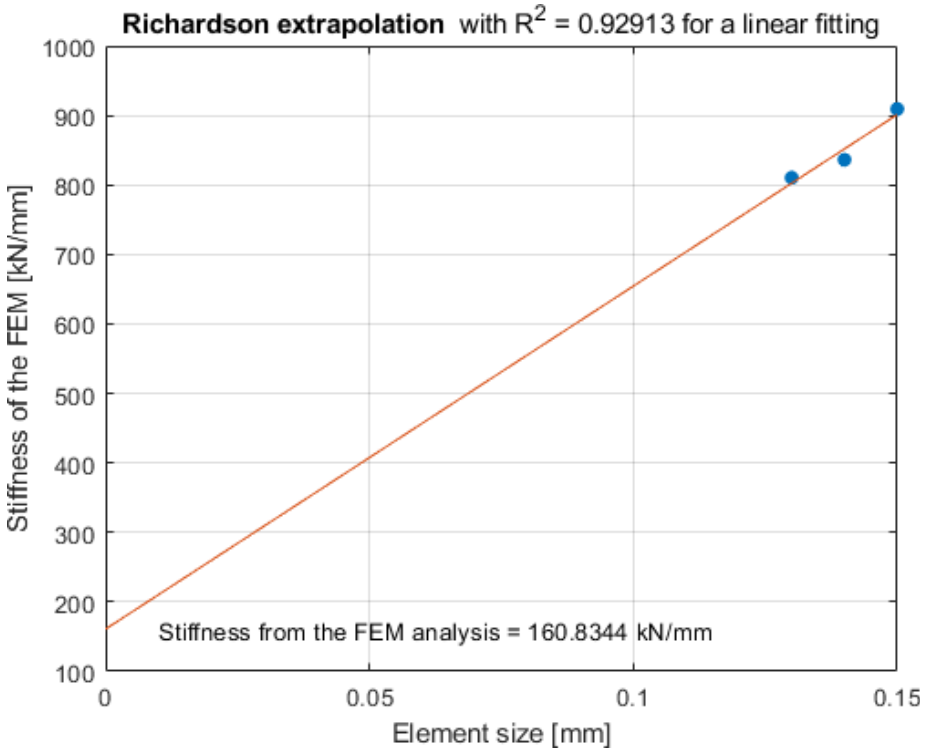

Figure 12. Richardson extrapolation for the 3D global model.

Comparing S(FEM) with the experimental stiffness S(Exp)= 192275 N/mm, it is possible to point out a difference of 16%. It is relevant to notice that this difference of 16% actually corresponds to the difference in BS: this is attributed to the partial contribution of the metallic powders in the closed cavities, making the compressive stiffness of SLM specimen to be higher.

In addition to this, for figuring out how the most stressed trabecula is loaded, a local reference system is defined by considering the axis of the trabecula and the orthogonal directions on its cross-section. The evaluation of the internal force and moment acting on the cross-section of the trabecula is highlighted in figure 13.

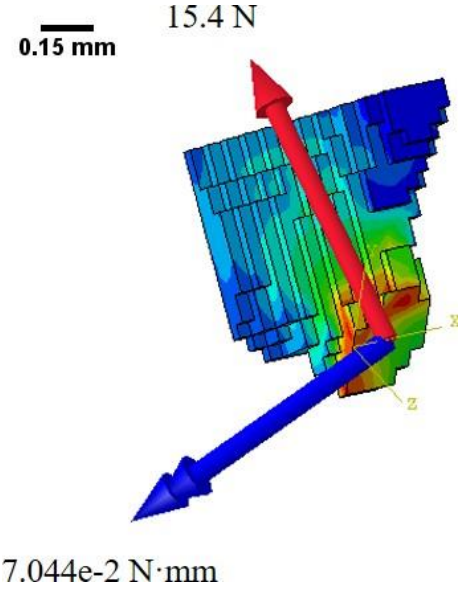

Figure 13. Internal forces acting on the trabecula.

It is interesting to observe that the trabecula mainly undergoes compressive load, that is crucial for damage initiation. Results discussed in [22] and [23] suggest that the trabecular structure damage is addressed by the zones with less material. However, even in that zones, collapse of the single trabeculae influences the failure of the global structure. In this context, future insights of the work will focus on exploiting the potentialities of the validated global model and the following sub-models, by varying the thickness of the trabecular network and isolating the effect of the geometry modification on the mechanical response to compressive loads. Further steps will explore the mechanical behavior of specimens in terms of the maximum deformation reached when the trabecular thickness is reduced. This is a hint to mimic the effect of bone pathologies, such as osteoporosis, that is characterized by a reduction in bone mineral density, completing the analysis of global parameters with local ones, such as local strains.

5. References

[1] Demontiero O, Vidal C and Duque G 2012 Aging and bone loss: New insights for the clinician *Ther. Adv. Musculoskelet. Dis.* **4** 61–76

[2] Raisz L G and Rodan G A 2003 Pathogenesis of osteoporosis *Endocrinol. Metab. Clin. North Am.* **32** 15–24

[3] Johnell O and Kanis J A 2006 An estimate of the worldwide prevalence and disability associated with osteoporotic fractures *Osteoporos. Int.* **17** 1726–33

[4] Klibanski A, Adams-Campbell L, Bassford T, Blair S N, Boden S D, Dickersin K, Gifford D R, Glasse L, Goldring S R, Hruska K, Johnson S R, McCauley L K and Russell W E 2001 Osteoporosis prevention, diagnosis, and therapy *Journal of the American Medical Association* vol 285 (American Medical Association) pp 785–95

[5] Sozen T, Ozisik L and Calik Basaran N 2017 An overview and management of osteoporosis *Eur.*

J. Rheumatol. **4** 46–56
[6] Akkawi I and Zmerly H 2018 Osteoporosis: Current concepts *Joints* **6** 122–7
[7] Gardner R L, Harris F, Vittinghoff E and Cummings S R 2008 The risk of fracture following hospitalization in older women and men *Arch. Intern. Med.* **168** 1671–7
[8] Marshall D, Johnell O and Wedel H 1996 Meta-analysis of how well measures of bone mineral density predict occurrence of osteoporotic fractures *Br. Med. J.* **312** 1254–9
[9] Hunt H B and Donnelly E 2016 Bone Quality Assessment Techniques: Geometric, Compositional, and Mechanical Characterization from Macroscale to Nanoscale *Clin. Rev. Bone Miner. Metab.* **14** 133–49
[10] Colombo C, Libonati F, Rinaudo L, Bellazzi M, Ulivieri F M and Vergani L 2019 A new finite element based parameter to predict bone fracture *PLoS One* **14**
[11] Mirzaali M J, Libonati F, Böhm C, Rinaudo L, Cesana B M, Ulivieri F M and Vergani L 2020 Fatigue-caused damage in trabecular bone from clinical, morphological and mechanical perspectives *Int. J. Fatigue* **133**
[12] Müller R and Rüegsegger P 1995 Three-dimensional finite element modelling of non-invasively assessed trabecular bone structures *Med. Eng. Phys.* **17** 126–33
[13] Crawford R P, Cann C E and Keaveny T M 2003 Finite element models predict in vitro vertebral body compressive strength better than quantitative computed tomography *Bone* **33** 744–50
[14] Barak M M and Black M A 2018 A novel use of 3D printing model demonstrates the effects of deteriorated trabecular bone structure on bone stiffness and strength *J. Mech. Behav. Biomed. Mater.* **78** 455–64
[15] Nagaraja S, Couse T L and Guldberg R E 2005 Trabecular bone microdamage and microstructural stresses under uniaxial compression *J. Biomech.* **38** 707–16
[16] Tassani S, Korfiatis V and Matsopoulos G K 2014 Influence of segmentation on micro-CT images of trabecular bone *J. Microsc.* **256** 75–81
[17] Saleh M A E and Ragab A E 2013 Ti-6Al-4V helical spring manufacturing via SLM: Effect of geometry on shear modulus *Lecture Notes in Engineering and Computer Science* vol 2203 (Newswood Limited) pp 950–3
[18] Burkhart T A, Andrews D M and Dunning C E 2013 Finite element modeling mesh quality, energy balance and validation methods: A review with recommendations associated with the modeling of bone tissue *J. Biomech.* **46** 1477–88
[19] Panjabi M and White A 1990 Clinical biomechanics of the spine
[20] Anon Robert; Cook, David Malkus, Michael Plesha, and Robert Witt. Concepts andApplications of Finite Element Analysis - Cerca con Google
[21] Ladd A J C and Kinney J H 1998 Numerical errors and uncertainties in finite-element modeling of trabecular bone *Journal of Biomechanics* vol 31 (Elsevier Sci Ltd) pp 941–5
[22] Nagaraja S, Couse T, biomechanics R G-J of and 2005 undefined Trabecular bone microdamage and microstructural stresses under uniaxial compression *Elsevier*
[23] Nazarian A, Stauber M, Zurakowski D, Bone B S- and 2006 undefined The interaction of microstructure and volume fraction in predicting failure in cancellous bone *Elsevier*

Acknowledgment
The author thanks the laboratory of CNR-ICMATE in Lecco (Italy) for the realization the SLM samples.